Phys. Status Solidi B **249,** No. 10, 1985–1991 (2012) / **DOI** 10.1002/pssb.201200419

physica status solidi b
www.pss-b.com
basic solid state physics

Part of Special Issue
Phase-change memory: Science and applications

Fast and scalable memory characteristics of Ge-doped SbTe phase change materials

Byung-ki Cheong*[,1], Suyoun Lee[1], Jeung-hyun Jeong[1], Sohee Park[2], Seungwu Han[2], Zhe Wu[3], and Dong-Ho Ahn[3]

[1] Electronic Materials Research Center, Korea Institute of Science and Technology, Seoul 136-791, Korea
[2] Department of Materials Science and Engineering, Seoul National University, Seoul 151-744, Korea
[3] Process Development Team, Semiconductor R&D Center, Samsung Electronics, Gyeonggi-Do 445-701, Korea

Received 23 June 2012, revised 11 August 2012, accepted 12 August 2012
Published online 19 September 2012

Dedicated to Stanford R. Ovshinsky on the occasion of his 90th birthday

Keywords Ge-doped SbTe, phase change memory, scalability, SET speed, storage class memory

* Corresponding author: e-mail bkcheong@kist.re.kr, Phone: +822-958-5385, Fax: +822-958-5409

Phase change memory (PCM) has opportunities of various applications on the premise of its high performance operations, which are still to develop with innovations such as change of a memory material. In respects of high-speed and high-scalability memory characteristics, δ-phase Ge-doped SbTe (GeST) materials stand as highly promising candidates. An overview of the material and device characteristics of these materials is presented primarily based on our recent experimental and computational studies and with a particular regard to their Sb-to-Te ratio (STR) dependence.

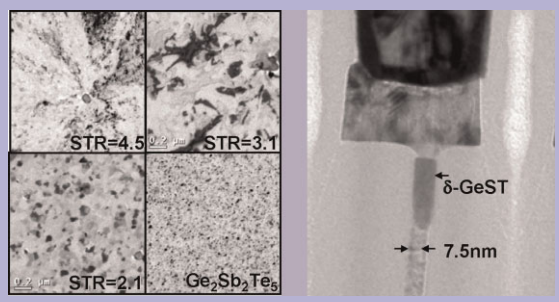

TEM images of the δ-phase GeST microstructures of varying STR and a highly scaled PCM cell with a δ-phase GeST of high STR.

1 Introduction Phase change memory (PCM) based on $Ge_2Sb_2Te_5$ (GST) material has been commercialized lately as NOR-replacements in mobile applications owing to its superior performance in writing speed and endurance as compared with NOR flash memory. Nevertheless, the GST-based PCM falls much short of the incumbent main stream memories, i.e. DRAM in speed and NAND in density and is not obviously up to the often stated PCM potential of being a universal memory. Meanwhile, PCM is considered as a strong candidate for so-called storage class memory (SCM) that is supposed to fill the performance gap in-between DRAM and SSD by providing DRAM-like speed on a SSD-like large storage capacity. At any rate, it seems evident that various projected opportunities of PCM may not be materialized unless significant-to-dramatic improvements are made in speed and density, for which use of a phase change material other than GST may be required.

As for speed of the GST-based PCM, a rather slow SET programming speed (about 300 ns) is of a particular concern. In this respect, it should be noted that a slow-quench preceded by melting is presently adopted in a commercial product as it turns out to be more effective than solid-state crystallization for obtaining a narrower distribution of SET resistance at an array level [1]. To expedite SET programming, therefore, crystallization should be completable with a faster quench and a material capable of a faster growth is better suited for the purpose. As for the scalability of PCM, it has been shown that employment of a damascene-type confined cell is very effective to reduce etch damages, inter-cell thermal interference, endurance failure and the RESET current as well [2]. ALD or CVD deposition of a phase change material should be adopted eventually.

With regard to these issues, doped SbTe materials seem to have much promise. Contrary to nucleation-dominated

crystallization of GST, the materials are featured by fast growth-dominated crystallization, which has been utilized for high-speed phase-change optical data storage based on mark-edge recording [3]. The potential of the materials as applied to electrical memory was first demonstrated using a phase-change line memory [4] but the subsequent studies have been rare along the same avenue. Using pore-type vertical devices and highly scaled devices, the present authors have recently carried out focused studies on the electrical memory characteristics of Ge-doped SbTe materials in respects of SET/RESET programming [5–7], multi-level programming [8], and reliable DRAM-like performance [9]. Herein, we put together these work in an overview of the materials' prospect for high performance memory as a dedication to this special issue for someone who initiated a path to the present day PCM forty some years ago. We start with a material perspective for Ge-doped SbTe that is relevant to discussions of the device characteristics to follow.

2 Material characteristics

2.1 Phase diagram characteristics Schematically shown in Fig. 1a is the calculated equilibrium phase diagram of Sb–Te binary system [10]. It consists of an Sb_2Te_3–Te portion of a simple eutectic-type and an Sb–Sb_2Te_3 portion with various invariant reactions. Between around 16 to 37 at% Te in particular, there exists the region of a stable single phase known as δ-phase with a congruent melting point at the Sb content of 72.3 at% and at the temperature 544.5°C. As shown in the Ge–$Sb_{69}Te_{31}$ pseudobinary section of Fig. 1b [11], Ge is soluble in the δ-phase of near the congruent composition up to slightly above 10 at%.

2.2 Composition dependence of crystalline/amorphous structures From a careful structural analysis of the Sb–Te materials of compositions belonging to the Sb–Sb_2Te_3 portion of the diagram, it was revealed that the crystal structures of the Sb–Te materials change with varying composition in such a manner that unit cell at a composition is composed of layers stacked according to ABC sequence where units of NaCl-type Sb_2Te_3 structure (Te–Sb–Te–Sb–Te layers) are interposed by A7-type Sb structure having varying number of Sb layers with composition [12]; any Sb–Te binary material belonging to the Sb–Sb_2Te_3 portion of the diagram may be viewed then essentially as a two phase (Sb + Sb_2Te_3) eutectic composite at the atomic level. It was suggested that a crystalline Sb–Te material in the Sb–Sb_2Te_3 portion may be expressed to have the chemical formula of $Sb_{2n}Te_3$ with a total of $2n+3$ stacked layers in its unit cell [12].

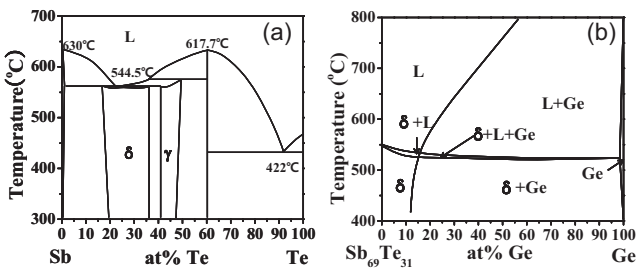

Figure 1 Equilibrium phase diagrams of (a) Sb–Te binary system and (b) $Sb_{69}Te_{31}$–Ge pseudo-binary system schematically reproduced from Refs. [10, 11].

Shown in Fig. 2a are the first-principles calculation results on the cystalline structures of three selected Sb–Te materials, i.e. $Sb_{2n}Te_3$ with $n=1$ and two δ-phase compositions with $n=3$ and 6. The details of computational methods can be found in Ref. [13]. It should be commented that each Sb atom within the stacked Sb layers has 3 short and 3 long near-orthogonal bonds with nearest neighbour Sb atoms but one within the Sb_2Te_3 substructures has rather symmetrical bonding with 6 Te atoms. Note also that weak Te–Te bonds across the two bounding layers in the c-Sb_2Te_3 stack are replaced with relatively stronger Te–Sb bonds in c-Sb_2Te and c-Sb_4Te, leading to increased atomic density of the latter. The calculated partial density of states (PDOS) for the three different crystalline structures are shown in Fig. 2b. With increasing Sb content, of band gap becomes reduced and the partial weight of Sb p band becomes stronger particularly near the top of valence band, rendering bonding orbitals predominantly the p-character. These changes appear to be pronounced from c-Sb_2Te_3 to c-Sb_2Te but not so significant from c-Sb_2Te to c-Sb_4Te, indicating a difference in bonding environments of Sb atom between c-Sb_2Te_3 and the others as mentioned above. From similarity in electronic structures between c-Sb_2Te and c-Sb_4Te, electrical and optical properties of δ-phase materials are expected to vary little with composition as confirmed experimentally by Sb–Te materials doped with 5 to 10 at% Ge [7, 14].

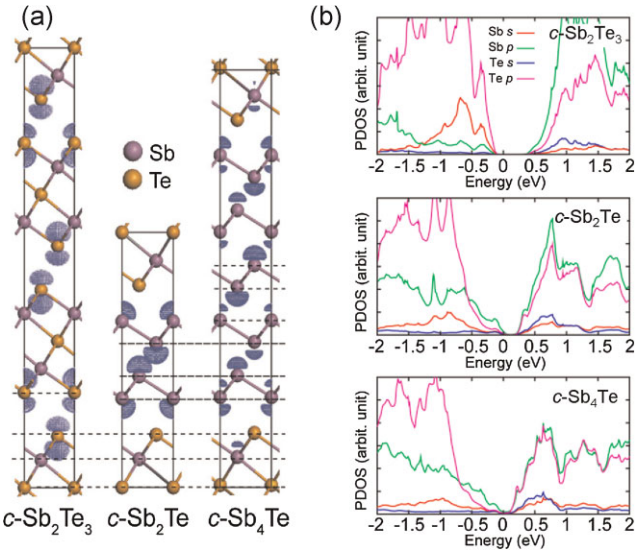

Figure 2 (online colour at: www.pss-b.com) (a) The hexagonal unit cell of c-Sb_2Te_3, c-Sb_2Te and c-Sb_4Te viewed along the (0001) axis. The contours are electron densities at the valence top and horizontal lines indicate the symmetrically independent layers. (b) The corresponding computed partial density of states (PDOS).

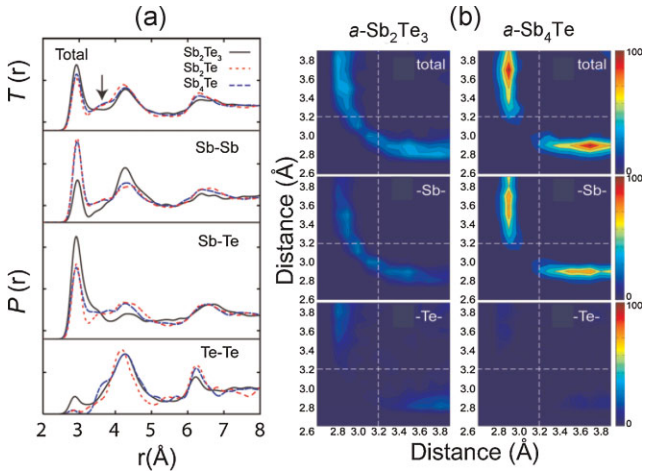

Figure 3 (online colour at: www.pss-b.com) (a) Radial distribution functions (RDF) of amorphous Sb_2Te_3, Sb_2Te and Sb_4Te. (b) Three-body correlation functions of amorphous Sb_2Te_3 and Sb_4Te.

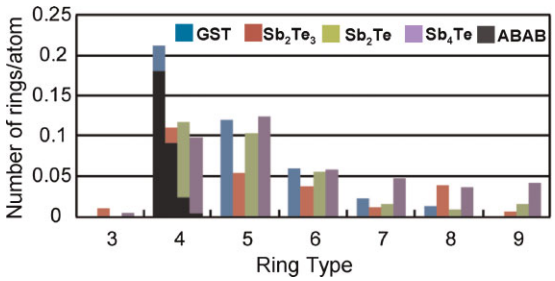

Figure 4 (online colour at: www.pss-b.com) Ring distributions in amorphous structures.

As for the amorphous Sb–Te materials of the three different compositions, the calculated radial distribution functions (RDF) are shown in Fig. 3a. Notice an apparent shoulder on the second peak at around 3.7 Å (marked by an arrow) for a-Sb_2Te and a-Sb_4Te, suggesting that the shoulder may be characteristic of local atomic structures in Sb-rich materials. A similar feature was also noted from the total correlation function of an amorphous $Ag_{3.5}In_{3.8}Sb_{75}Te_{17}$ (AIST) alloy [15]. For a detailed analysis, we mapped out three-body correlation functions in Fig. 3b representing the distribution of bond lengths in three-atom alignments of two bonds having inter-bond angles in the range of 140° to 180°. Regarding the shoulder on the second peak in RDF, notice that a-Sb_4Te has a bond distribution characterized by prominently lineal three-atom alignment with one short bond (∼2.9 Å) and one long bond (∼3.7 Å) relative to that of a-Sb_2Te_3. Since such three-atom alignment constitutes a crystalline structural motif, it may transform into a locally ordered arrangement with a small displacement of an Sb atom, hence crystallization of Sb-rich materials being a growth-controlled process. According to an atomistic model derived from careful analyses of the atomic and electronic structures of the amorphous and crystalline AIST alloys, growth-dominated crystallization proceeds by successive bond interchanges through small displacements of Sb atoms in $3+3$ octahedra along the crystalline c-axis imposed by the surrounding crystal [15]. It is readily expected that the process would be most rapid in the pure Sb case and the presence of other elements may impede it, leading to decreased growth speed.

The composition dependence of the medium range order in amorphous state as examined by the ring distributions is shown in Fig. 4. It is noted that Sb–Te materials have broader size distributions than GST and a-Sb_4Te in particular shows a stretched ring distribution with fivefold rings being the largest in number. As for fourfold rings, notice that AAAB-type (A; Ge, Sb, B; Te) is predominant in a-Sb_2Te and a-Sb_4Te whereas ABAB-type is so in a-GST and a-Sb_2Te_3. This seems to explain the difference in crystallization mode between the two groups of materials. Unlikely to be sustainable during electrical or optical heating, weakly bonded AAAB-type rings may not contribute to nucleation-dominated crystallization as ABAB-type fourfold rings do in GST and possibly in a-Sb_2Te_3.

Regarding the effect of Ge-doping on the structures of Sb–Te materials, a few comments are in order. Firstly, Ge addition increases the average mean coordination number of an amorphous material, thereby increasing the thermal stability of an amorphous phase [16, 17]. As for crystalline structures, Ge addition beyond a certain content appears to make changes in stable crystalline structures. For example, laser-crystallized $Ge_{7.1}Sb_{76.4}Te_{16.5}$ material was found to have A7-type crystal structure at room temperature and even a simple cubic at high temperatures [18] whereas Sb–Te doped with as small as 5 at% Ge were observed to maintain the aforestated long period stacked structures [14].

2.3 Composition dependence of crystallization kinetics Shown in Fig. 5 are the nucleation and growth kinetics of Sb–Te materials doped with about 5 at%Ge or less as measured by two separate groups using laser crystallization [5, 19]. Between the two groups' data, there is no

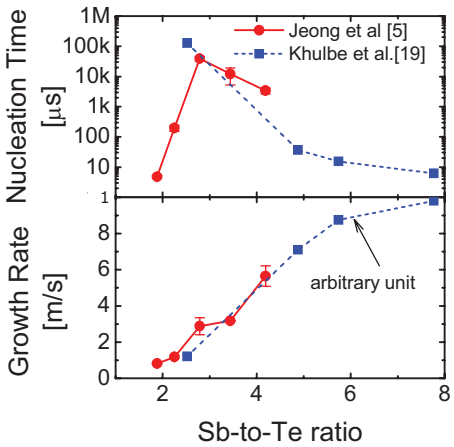

Figure 5 (online colour at: www.pss-b.com) Crystallization kinetics as measured by laser annealing of Ge-doped SbTe films of varying STR [5, 19].

discrepancy in displaying a monotonous increase of growth speed with increasing Sb to Te ratio (STR), in line with the foregoing discussions. As for nucleation time, two remarkable features are found from measurements over an extended range of STR down to the Sb-lean side of the δ-phase boundary (STR of ∼1.7). Firstly, nucleation time reaches a maximum near the minimum congruent melting point (STR of 2.6) where the driving force for crystallization is supposedly smaller than in adjacent compositions. From classical nucleation theory, crystallization is expected to require the largest viable nuclei hence the longest nucleation time at the congruent composition, provided that the interface energy of a nucleus varies little over a small range of composition. Secondly, nucleation time becomes drastically reduced with STR decreasing from the congruent composition and enters the submicron-second regime hence most likely the regime of nucleation-dominated crystallization as the Sb-lean side of the δ-phase boundary is crossed. Note that the two characteristic compositions (STR of 2.6 and 1.7) are corresponding to Sb_8Te_3 and Sb_5Te_3 crystalline structures, respectively. Remarkably, a unit cell of an Sb phase can barely form within the interposed Sb layers of the former structure and an Sb-based three-atom alignment, a motif of a crystalline Sb, can barely form in the latter.

3 Programming characteristics Shown in Fig. 6 is the composition dependence of the SET and RESET programming characteristics, as examined with PCM cells having the pore size of 150 nm × 150 nm and $Ge_{10}ST$ materials of varying STR; 10 at%Ge was added for improved thermal stability of the materials. The detailed procedures of device fabrication and characterization can be found in Ref. [6, 7]. From Fig. 6a, each of R_{RESET}, R_{SET} and V_{th} is found to decrease rather monotonously with STR, similar to a trend displayed by the electrical resistivity data (not shown here). The results for two important device characteristics, SET time (t_{SET}) and RESET current (I_{RESET}), are shown in Fig. 6b together with two elements of t_{SET}, i.e. delay time (t_D) and crystallization time (t_{Cryst}). Notice a very short t_{SET} of around 30 ns at the highest STR tested and a slow increase with decreasing STR down to about 1.7 before a steep rise in the range of still lower STRs. Such a characteristic trend is observed to inherit from that of crystallization time that appears to come from a qualitative change in crystallization

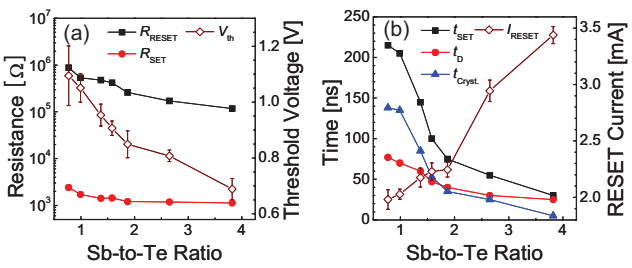

Figure 6 (online colour at: www.pss-b.com) (a) R_{RESET}, R_{SET}, and V_{th}, (b) I_{RESET} and t_{SET} as a function of STR.

Table 1 Selected material parameters of three different δ-phase Ge-doped SbTe materials; $Ge_{10}ST_L$ ($Ge_{9.9}Sb_{57.9}Te_{32.2}$), $Ge_{10}ST_M$ ($Ge_{9.9}Sb_{65.4}Te_{24.7}$), $Ge_{10}ST_H$ ($Ge_{9.9}Sb_{71.4}Te_{18.7}$).

	$Ge_{10}ST_L$	$Ge_{10}ST_M$	$Ge_{10}ST_H$
T_m (°C)	∼544	∼544	∼544
$\rho_{cryst.}$ (Ω.cm)	3.7×10^{-4}	2.7×10^{-4}	3.8×10^{-4}
$\Lambda_{cryst.}$(W mK^{-1})	4.8	5.0	4.5
V_{growth} (m s^{-1})	0.8	∼3.6	∼5.9

mode across the δ-phase boundary most likely from a growth-dominated mode to nucleation-dominated one. A distinctively contrasting trend is observed for I_{RESET}, namely, a steep decrease from its maximum with diminishing STR down to the δ-phase boundary and a markedly slower decrease therefrom to STR of about 0.7. To understand the origin of the observed trends in hindsight, relevant material parameters are listed in Table 1 for three selected compositions of the δ-phase [7]. Note that the first three sets of material parameters differ little among the three selected compositions, being explainable by the similarity of the local atomic and electronic structures as indicated above.

Indeed, electrothermal calculations taking account of only the first three sets of material parameters were found to yield I_{RESET} values having positive deviations progressively from the observed values with growing STR, implying an increasingly adverse role of V_{growth} in determining I_{RESET} of the higher STR material. It was confirmed that V_{growth} has a remarkable influence on the RESET programming process by modulating the regrowth kinetics of the crystals surrounding the molten programming region during the quenching period [7]. In as much as both RESET- and SET-programming characteristics are governed by the regrowth kinetics of the surrounding crystals, I_{RESET} and t_{SET} are inseparably linked as competing performance parameters and a judicious choice of the STR is deemed necessary depending on the target application.

Another ramification of the problem with fast regrowth stands out in MLC programming. MLC programming with a growth-dominated PCM material in particular requires an accurate control of the size of an amorphous programmed region so as to produce multiple resistance levels reliably. For a δ-phase material with a high STR, this appears to be quite challenging due to very rapid regrowth kinetics and MLC programming has been pursued instead by polarity reversal [20] for instance. With a δ-phase material of a reduced STR, MLC programming capability can be imparted to a PCM cell as shown in Fig. 7 [8]. It is observed from Fig. 7a that the material ($GeST_L$) with a relatively low STR (1.8) produces more gradual change in resistance from SET to RESET states as falling time (t_f) of a programming pulse increases from 5 to 20 ns whereas the other two materials of higher STRs maintain the abrupt resistance changes with concurrent rises in RESET current. This indicates that amorphous regions of varying sizes are able to form by current modulation owing to the reduced regrowth kinetics

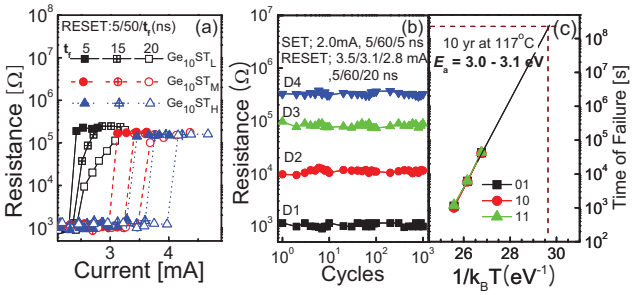

Figure 7 (online colour at: www.pss-b.com) (a) *I–R* characteristics of memory cells using $Ge_{10}ST_L$, $Ge_{10}ST_M$ and $Ge_{10}ST_H$, (b) cyclic 4-level programming, (c) data retention characteristics of the MLC-$Ge_{10}ST_L$ cell.

of the $GeST_L$ material. As shown in Fig. 7b and c, four-levels of resistance were programmable reproducibly with relatively short SET (5/60/5 ns; rising time/pulse width/falling time, respectively) and RESET (5/60/20 ns) pulses and could be maintained stable for 10 years at 117 °C. It follows that δ-phase $GeST_L$ looks also promising besides a high STR material as it provides relatively low reset current and MLC capability without much sacrifice of SET speed.

4 Characteristics of highly scaled device Needless to say, a good scalability must be warranted for practical use of a δ-phase GeST material. According to International Technology Roadmap for Semiconductor (ITRS) 2011, reset current value of PCM is expected to reach below 100 μA at 20 nm technology node (Fig. 8a). As shown in Fig. 8b, the aspect ratio of a storage node (that can be determined from the cross-sectional area of a phase change volume in ITRS 2011 with an assumed anisotropic device scaling for reset current) is predicted to increase rapidly from this node down on [21, 22].

It is very challenging to form a phase change material with a high aspect ratio of more than 4 using a conventional physical vapor deposition (PVD) technique combined with an etching process without producing gap-fill voids and etch damages. Figure 9 shows the evolution of the cell structure with its compatible deposition process [2, 23, 24]. Control of etch damages with the conventional processes was not much of an issue down to the technology node of about 60 nm.

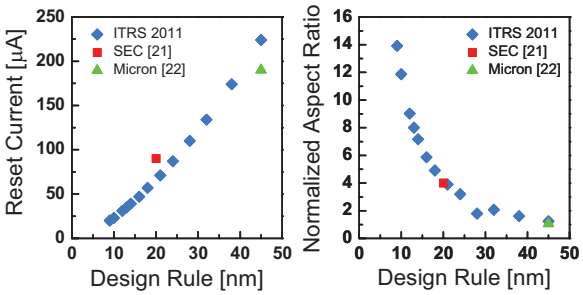

Figure 8 (online colour at: www.pss-b.com) Estimated reset current and aspect ratio of a PCM storage node as a function of design rule; experimental results are also included.

Cell Structure	Planar-type [23]	Damascene-type [2]	Dash-type [24]
Cross-sectional TEM Micrographs		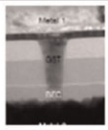	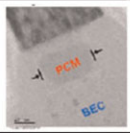
Dep. Process	PVD	CVD	ALD

Figure 9 (online colour at: www.pss-b.com) Evolution of PCM cell structure (from left to right) with the compatible deposition process.

Below 60 nm node, a CVD process was introduced to fill a trench hole whilst a CMP process replacing the etching process. Eventually an isolated dash-type cell was developed together with ALD process to enable a conformal filling of a tiny contact hole. Recent reports from two different research groups address the issues of CVD/ALD precursors and deposition processes for various phase change materials including GeST materials [25, 26].

A dash-type cell containing a GeST of a high STR inside a trench hole of 7.5 nm × 17 nm in size was fabricated using an ALD process as shown in Fig. 10 and was characterized with respect to various memory characteristics [9]. The measured SET speed and data retention characteristics of the GeST dash-type cell are presented in Fig. 11 showing a SET speed of 30 ns and the estimated retention times of 4.5 years at 85 °C and of over 10 years at 70 °C, respectively. Evidently, these characteristics fulfill the requirements of SCM [27]. The observed SET speed is slightly slower than that of the planar-type cell, which is supposedly due to the

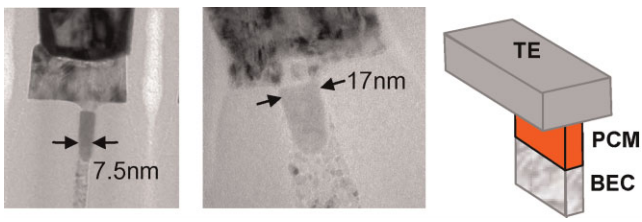

Figure 10 (online colour at: www.pss-b.com) Dash-type PCM cell with a δ-GeST of a high STR.

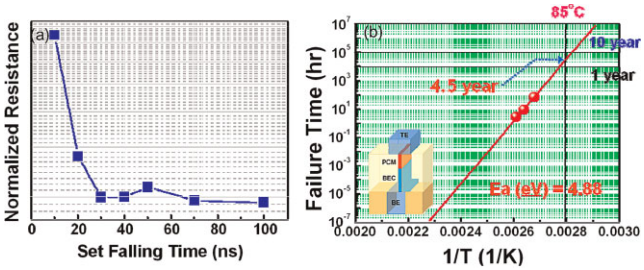

Figure 11 (online colour at: www.pss-b.com) (a) SET resistance characteristic as a function of SET pulse time and (b) Arrhenius plot of data retention time as a function of temperature for a δ-GeST dash-type cell.

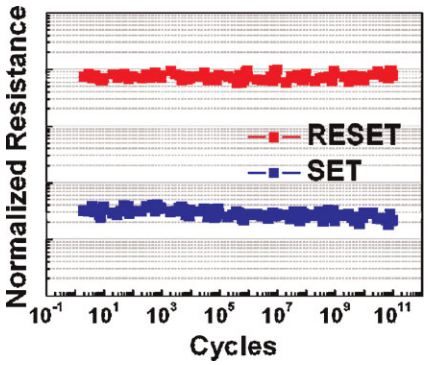

Figure 12 (online colour at: www.pss-b.com) Endurance characteristic of a δ-GeST dash-type cell.

relative deficiency of a crystalline matrix around an amorphous volume in the isolated dash-type cell. Consistent with this, data retention characteristics of the dash-type cell are also relatively better.

One of the most important requirements for the SCM is a long cyclability of 10^{9}–10^{12}. In the case of PRAM for NOR replacement, endurance of 10^{4}–10^{5} was required, which could be easily satisfied with a control of dopants in a phase change material or by reset energy reduction. Endurance failures are well known to result from compositional segregation and voiding by way of atomic transport induced by the bias-dependent electro-migration in the molten GST and/or incongruent melting occurring at the boundary region between liquid and solid [28, 29]. An isolated confined cell can inhibit the endurance failure by reducing the reservoir for atomic transport and the solid/liquid boundary region as well. The GeST dash-type cell was capable of 10^{11} endurance cycles of writing operations as shown in Fig. 12.

5 Conclusion In order to satisfy the requirements of various high-end applications, PCM needs to have improved performance in terms of speed and density. For enhanced speed in particular, a material seems in need, different from GST in present use. The δ-phase GeST materials offer a range of device characteristics that may be tailored to the specific needs based on a faster writing speed than GST. As a good example, GeST of a high STR can provide the speed, scalability and reliability required for the SCM application.

Acknowledgements We would like to acknowledge research grants from Korean Ministry of Knowledge Economy, Republic of Korea via National Research Program for 0.1 Terabit Nonvolatile Memory Devices and also Fundamental R&D Program for Core Technology of Materials. The computations were carried out at KISTI (No. KSC-2011-C3-17).

References

[1] K.-J. Lee, B.-H. Cho, W.-Y. Cho, S. Kang, B.-G. Choi, H.-R. Oh, C.-S. Lee, H.-J. Kim, J.-M. Park, Q. Wang, M.-H. Park, Y.-H. Ro, J.-Y. Choi, K.-S. Kim, Y.-R. Kim, I.-C. Shin, K.-W. Lim, H.-K. Cho, C.-H. Choi, W.-R. Chung, D.-E. Kim, K.-S. Yu, G.-T. Jeong, H.-S. Jeong, C.-K. Kwak, C.-H. Kim, and K. Kim, IEEE J. Solid-State Circuits **43**, 150 (2008).

[2] J. I. Lee, H. Park, S. L. Cho, Y. L. Park, B. J. Bae, J. H. Park, J. S. Park, H. G. An, J. S. Bae, D. H. Ahn, Y. T. Kim, H. Horii, S. A. Song, J. C. Shin, S. O. Park, H. S. Kim, U. In Chung, J. T. Moon, and B. I. Ryu, Dig. Tech. Pap. Symp. VLSI Technol., 2007, pp. 102–103.

[3] H. J. Borg, M. V. Schijndel, J. C. N. Rijpers, and M. H. R. Lankhorst, Jpn. J. Appl. Phys. **40**, 1592 (2001).

[4] M. H. R. Lankhorst, B. W. S. M. M. Ketelaars, and R. A. M. Wolters, Nature Mater. **4**, 347 (2005).

[5] J. H. Jeong, H. S. Lee, S. Y. Lee, T. S. Lee, W. M. Kim, Z. Wu, S. C. Kim, K. H. Oh, and B. Cheong, J. Phys. D, Appl. Phys. **42**, 035104-1 (2009).

[6] S. Lee, J. H. Jeong, Z. Wu, Y. W. Park, W. M. Kim, and B. Cheong, J. Electrochem. Soc. **156**, H612 (2009).

[7] Z. Wu, G. Zang, Y. W. Park, S. D. Kang, H.-K. Lyeo, D. S. Jeong, J. H. Jeong, K. No, and B. Cheong, Appl. Phys. Lett. **99**, 143505-1 (2011).

[8] G. Zhang, Z. Wu, J. H. Jeong, D. S. Jeong, W. J. Yoo, and B. Cheong, Curr. Appl. Phys. **11**, e79 (2011).

[9] I. S. Kim, S. L. Cho, D. H. Im, E. H. Cho, D. H. Kim, G. H. Oh, D. H. Ahn, S. O. Park, S. W. Nam, J. T. Moon, and C. H. Chung, Dig. Tech. Pap. Symp. VLSI Technol., 2010, pp. 203–204.

[10] G. Ghosh, J. Phase Equilib. **15**, 239 (1994).

[11] S. Bordas, M. T. Calvaguera-Mora, B. Legendre, and C. Hancheng, Thermochim. Acta **107**, 239 (1986).

[12] K. Kifune, Y. Kuita, T. Matsunaga, and N. Yamada, Acta Crystallogr. **61**, 492 (2005).

[13] E. Cho, Y. Youn, and S. Han, Appl. Phys. Lett. **99**, 183501 (2011).

[14] T. D. Kang, A. Sirenko, J. W. Park, H. S. Lee, S. Lee, J. H. Jeong, B. Cheong, and H. Lee, J. Electrochem. Soc. **158**, H249 (2011).

[15] T. Matsunaga, J. Akola, S. Kohara, T. Honma, K. Kobayashi, E. Ikenaga, R. O. Jones, N. Yamada, M. Takata, and R. Kojima, Nature Mater. **10**, 129 (2011).

[16] E. Prokhorov, J. Gonzalez-Hernandez, A. Mendoza-Galvan, G. Trapaga, and G. Luna-Barcenas, J. Non-Cryst. Solids **357**, 1610 (2011).

[17] L. Van Pieterson, M. H. R. Lankhorst, M. Van Schijndel, A. E. T. Juiper, and J. H. J. Roosen, J. Appl. Phys. **97**, 083520 (2005).

[18] T. Matsunaga and N. Yamada, Jpn. J. Appl. Phys. **43**, 4704 (2004).

[19] P. K. Kulbe, T. Hurst, M. Horie, and M. Masuripur, Appl. Opt. **41**, 6220 (2002).

[20] S. Lee, J. H. Jeong, T. S. Lee, W. M. Kim, and B. Cheong, Appl. Phys. Lett. **92**, 243507 (2008).

[21] M. J. Kang, T. J. Park, Y. W. Kwon, D. H. Ahn, Y. S. Kang, H. Jeong, S. J. Ahn, Y. J. Song, B. C. Kim, S. W. Nam, H. K. Kang, G. T. Jeong, and C. H. Chung, Tech. Dig. IEEE Int. Electron Device Meeting, 2011, pp. 39–42.

[22] G. Servalli, Tech. Dig. IEEE Int. Electron Device Meeting, 2009, pp. 113–116.

[23] S. L. Cho, J. H. Yi, Y. H. Ha, B. J. Kuh, C. M. Lee, J. H. Park, S. D. Nam, H. Horii, B. O. Cho, K. C. Ryoo, S. O. Park, H. S. Kim, U-In Chung, J. T. Moon, and B. I. Ryu, Dig. Tech. Pap. Symp. VLSI Technol., 2005, pp. 96–97.

[24] D. H. Im, J. I. Lee, S. L. Cho, H. G. An, D. H. Kim, I. S. Kim, H. Park, D. H. Ahn, H. Horii, S. O. Park, U-In Chung, and J. T. Moon, Tech. Dig. IEEE Int. Electron Device Meeting, 2008, pp. 211–214.
[25] M. Ritala, V. Pore, T. Hatanpaa, M. Heikkila, M. Leskela, K. Mizohata, A. Schrott, S. Raoux, and S. M. Rossnagel, Microelectron. Eng. **86**, 1946 (2009).
[26] S. Choi, B. J. Choi, T. Eom, J. H. Jang, W. Lee, and C. S. Hwang, J. Phys. Chem. C **114**, 17899–17904 (2010).
[27] G. W. Burr, B. N. Kurdi, J. C. Scott, C. H. Lam, K. Gopalakrishnan, and R. S. Shenoy, IBM J. Res. Dev. **52**, 449 (2008).
[28] J. S. Bae, K. M. Hwang, K. H. Park, S. B. Jeon, J. Choi, J. H. Ahn, S. S. Kim, D. H. Ahn, H. S. Jeong, S. W. Nam, G. T. Jeong, and H. K. Cho, Tech. Dig. IEEE Int. Reliab. Phys. Symp., 2012, EM.7.1–EM.7.4.
[29] S. J. Ahn, H. Jeong, B. Kim, Y. S. Kang, Y. Song, D. H. Ahn, S. W. Nam, H. K. Kang, G. Jeong, and C. Chung, Tech. Dig. IEEE Int. Electron Device Meeting, 2011, pp. 12.6.1–12.6.4.